Pergamon

Int. J. Solids Structures Vol. 35, Nos. 5–6, pp. 487–509, 1998

0020–7683/98 $19.00 + .00

PII: S0020–7683(97)00031–0

THE SLIDING CRACK MODEL OF BRITTLE DEFORMATION: AN INTERNAL VARIABLE APPROACH

M. BASISTA† and D. GROSS
Institute of Mechanics, TH Darmstadt, Hochschulstrasse 1, 64289 Darmstadt, Germany

(*Received* 28 *December* 1995; *in revised form* 20 *December* 1996)

Abstract—Rice's internal variable theory including a micro-to-macro transition is employed to formulate a micromechanical, two-dimensional damage model of brittle deformation in compression. The sliding crack model is selected as a basic dissipative mechanism underlying macroscopic inelastic deformation. Microfluxes and conjugated thermodynamic forces are identified and incremental stress–strain relations are derived in loading and unloading. Comparison with the model of Nemat-Nasser and Obata (Nemat-Nasser, S. and Obata, M. (1988) A microcrack model of dilatancy in brittle materials. *Journal of Applied Mechanics* **55**, 24–35, in which the sliding crack mechanism was analyzed from a kinematic point of view, is presented. An illustrative example is worked out showing the capability of the present model to predict experimentally observed response of a compact rock. © 1997 Elsevier Science Ltd.

1. INTRODUCTION

Heterogeneous brittle materials such as polycrystalline rocks and ceramics exhibit a very complex and nonlinear overall response when subjected to compressive loads. The most characteristic features observed in the deformation process of low-porosity rocks include (cf. Brace *et al.* 1966; Peng and Johnson, 1972; Zoback and Byerlee, 1975):

- threshold-type deviation from a linear elastic behavior accompanied by a gradual degradation of elastic constants,
- strong influence of confining pressures on the ultimate strength and failure modes (splitting, faulting, brittle-ductile transition),
- positive dilatancy, i.e., nonlinear volume increase due to opening of axial cracks (an initial concave shape of the stress–strain curve is commonly attributed to the closure of some preexisting pores and cracks),
- load-induced anisotropy ensuing from a directional process of microcrack evolution,
- hysteresis loops observed in the stress–strain curves in a loading–unloading–reloading cycle,
- pronounced permanent volumetric strain after complete unloading; little permanent strain in the direction of maximum compression (axial),
- strain softening regime beyond the peak in the stress–strain curves in strain-controlled tests.

On the basis of microscopic studies, several possible cracking mechanisms were identified to be responsible for the inelastic behavior and failure of rocks in compression (Kemeny and Cook, 1991). Among these mechanisms, two were given special attention in the relevant literature: (1) axial tensile microcracks emanating from pores, cavities, and/or inclusions that serve as stress concentrators for local splitting stresses (Sammis and Ashby, 1986), (2) frictional sliding on preexisting closed flaws coupled with an out-of-plane growth of secondary tension cracks (Horii and Nemat-Nasser, 1985). The sliding crack model with cohesive and frictional resistance seems to capture most of the above listed characteristics of the pre-peak response of rocks under compressive stresses. Apparently, it is for this versatility that the sliding crack mechanism, originated by Brace and Bombolakis (1963),

† Permanent address: Institute of Fundamental Technological Research, Swietokrzyska 21, 00-049 Warsaw, Poland.

was so widely used in rock mechanics (see, for example, Scholz and Kranz, 1974; Brace *et al.*, 1966; Zoback and Byerlee, 1975; Nemat-Nasser and Horii, 1982; Horii and Nemat-Nasser, 1985, 1986), and damage mechanics (Kachanov, 1982, 1993; Moss and Gupta, 1982; Ashby and Hallam, 1986, Nemat-Nasser and Obata, 1988; Deng and Nemat-Nasser, 1994; Sadowski, 1994). However, there is a continuing debate in the open literature whether the sliding crack mechanism actually appears in *real* brittle materials. It has been argued by some authors that SEM observations do not support the existence of winged microcracks, but seem to favor a complex configuration of tensile microcracks propagating from different sources. On the other hand, recent data from acoustic emission tests do indicate that both tensile and shear events occur during brittle rock deformation (Lockner, 1993; Zhang *et al.*, 1996). In our opinion, for compact and relatively homogeneous rocks such as granite, the sliding crack mechanism should be considered as, at least, one of the major micromechanisms of inelastic deformation. It is clear, though, that more sophisticated experimental techniques and the problem-oriented experimental programs are still necessary to resolve this controversy.

A majority of micromechanical damage models follow a *kinematic* algorithm for the computation of inelastic strains. A common assumption is made in these models that straight slits or penny-shaped cracks grow in a self-similar manner. The inelastic part of the strain tensor $\boldsymbol{\varepsilon}^i$ is typically written in terms of a dyadic product of the displacement jump vector $\mathbf{b}$ (CODs), and the vector $\mathbf{n}$ normal to the crack surface:

$$\boldsymbol{\varepsilon}^i = \frac{1}{2V_0}\int_{A_{(k)}} (\mathbf{n}\otimes\mathbf{b}+\mathbf{b}\otimes\mathbf{n})\,\mathrm{d}A. \tag{1}$$

Here V_0 is the volume of a statistically representative sample of material in unloaded reference state, and $A_{(k)}$ denotes the area of k-th crack. In a two-dimensional case, V_0 and $A_{(k)}$ should be replaced by the area of a representative surface element A_0 and the length of a crack $2l_{(k)}$, respectively. Since CODs are linear functions of stresses, $\boldsymbol{\varepsilon}^i$ defined in eqn (1) can also be represented using the inelastic secant (effective) compliance tensor as $\boldsymbol{\varepsilon}^i = \tilde{\mathbf{S}}^i : \boldsymbol{\sigma}$. The microcrack interaction effects are either ignored (Taylor model) or accounted for in a simplified manner through one of the effective medium techniques. For example, within the context of the self-consistent method, we have to determine the crack opening displacements $\mathbf{b}$ of an isolated crack embedded in effective anisotropic matrix of as yet unknown elastic moduli. Closed-form solutions for the CODs are available in the literature for open straight (or penny-shaped) cracks under Mode I or mixed I/II Mode conditions in an homogeneous anisotropic elastic solid. These solutions involve the roots of the characteristic equation which follows from the geometric compatibility condition (for details, see Ju, 1991). As a direct consequence of the self-consistency, an iterative scheme is required to determine damage-related components of the compliance tensor. The same procedure can be extended to closed microcracks under Mode II frictional sliding (Nemat-Nasser and Horii, 1983; Sumarac and Krajcinovic, 1987).

On the other hand, Nemat-Nasser and Obata (1988) presented a rigorous 2D micromechanical constitutive model for brittle materials under compression, in which the restrictive assumption of a self-similar crack evolution was relaxed. These authors incorporated the sliding crack mechanism as a main building block of their model. On the basis of (1), they derived complete nonlinear stress–strain relations in loading and unloading regimes. The preexisting crack was endowed with frictional and cohesive resistance. However, the microcrack interaction and, therefore, the final failure was not considered.

In this paper, we shall re-examine the sliding crack mechanism from a different viewpoint, namely within the general thermodynamic framework of Rice (1971, 1975) which rests on the concept of internal variables. The basic kinematic relation (1) will not be used for the computation of strains. Instead, increments of the macroscopic strain tensor will be derived using the Rice *micro-to-macro* transition. Although macroscopic internal variables (damage parameters) are often used in phenomenological modeling of damaged solids, a natural combination of an internal variable formulation with micromechanics of damage

processes has not been fully explored. At least, the sliding crack mechanism seems not to have been analyzed this way. The primary objective here is to relate specific structural rearrangements on the microscale (frictional sliding and/or wing cracking) to the inelastic macroscopic deformation of the representative volume element. In other words, the forms of the potential functions will not be just postulated but will be derived from micromechanics. The emphasis will be placed on qualitative results. Consequently, it seems justified to consider a two-dimensional model with the winged crack of a simplified geometry. Clearly, this approach is dual to the 2D kinematic analysis by Nemat-Nasser and Obata (1988). Therefore, a comparison of the results furnished by both models will be presented.

2. FORMULATION

Consider an isothermal deformation process of an elastic solid such as rock weakened by a large number of dilutely distributed initial microcracks. Assume strains to be infinitesimal and confining pressures to remain moderate so that typical plastic effects, observed in brittle materials at high lateral pressures, can be neglected. Assume further that damage develops from the preexisting defects and no new microcrack nucleation is allowed in the course of deformation. These assumptions are pertinent to *cleavage* 1 type of deformation in Ashby's classification (Ashby, 1979). Microcrack interactions are not examined here and will be commented upon in Section 4. To make the analysis tractable, select a representative initial microcrack as a single, closed rectilinear slit PP' of the length $2c$ oriented at an angle φ, as depicted in Fig. 1. This microcrack is embedded in a two-dimensional, elastically isotropic, homogeneous unbounded matrix loaded under plane strain conditions. The sign convention is that of continuum mechanics, i.e., compressive stresses are viewed negative. Moreover, it is chosen that $|\sigma_1| > |\sigma_2|$. Two Cartesian coordinate systems will be used throughout the paper: a fixed global frame of reference (x_1, x_2) and a local one (x_1', x_2'), Fig. 1.

The onset of macroscopic inelastic deformation in brittle rocks is typically attributed to the activation of frictional sliding over the faces of preexisting microcracks†. During this phase, called *phase* 1 in the sequel, the cracks retain their length $2c$, thus no new internal surfaces are created (no wings yet). The only energy dissipating mechanism is the frictional sliding in the shearing mode. It is also assumed that the inclined preexisting crack remains closed during the whole deformation process. Phase 1 is characterized by a trigger-like

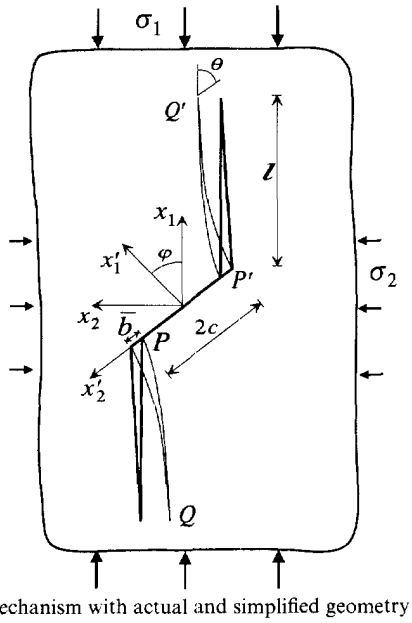

Fig. 1. Sliding crack mechanism with actual and simplified geometry of tensile wing cracks.

† Nonlinear strains induced by the initial closure of pores are here neglected.

kinetics, i.e. sliding commences when the actual shear stress acting on the crack faces overcomes the combined resistance of friction, cohesion and that of elastic crack-restoring forces. Once the sliding is activated, the representative crack is in Mode II loading for which only K_{II} stress intensity factor is nonzero. At some point, the elastic energy release rate $G(\theta)$ of an infinitesimal kink tip will reach a critical value in a plane at an angle θ_c to the original crack. The critical value of G corresponds to the critical value of the tensile hoop stress $\sigma_{\theta\theta}$ in the vicinity of the crack tip. Regardless of interpretation, the original crack will abruptly sprout a curvilinear wing (kink) crack at each tip at $\theta_c = 70.5°$, Fig. 1. According to the linear fracture mechanics solution, the crack tip will follow a path for which $K_I = \max$, or equivalently, $K_{II} = 0$. After a short initial curving, the wings will align themselves with the direction of maximum principal compression σ_1 and become rather straight. The exact trajectory of the wing tip can be determined by maximizing $\sigma_{\theta\theta}$ with respect to θ. In this phase, called *phase* 2, the inelastic strains result from the coupled effects of frictional sliding along PP' and opening of the wings cracks PQ and $P'Q'$. In what follows, we shall derive the stress–strain relations for each phase separately. But before we do this, it is advisable to interpret the Rice theory in the context of the sliding crack mechanism.

2.1. *Rice's framework in case of frictional cracks*

The envisaged constitutive model will be formulated within the thermodynamic framework with internal variables as developed in Kestin and Rice (1970), Rice (1971, 1975), Hill and Rice (1973). To keep the analysis self-contained, the essential structure of this theory is briefly described in Appendix 1. Here, we recall only the fundamental Rice transition relation that provides a recipe how to compute macroscopic inelastic strain from its microstructural origins, namely

$$\mathrm{d}^i\varepsilon_{ij} = \frac{1}{V_0}\sum \frac{\partial f_\alpha(\boldsymbol{\sigma}, H)}{\partial \sigma_{ij}}\mathrm{d}\xi_\alpha, \tag{2}$$

where $f_\alpha = f_\alpha(\boldsymbol{\sigma}, H)$ is a set of thermodynamic forces conjugated to the internal variables ξ_α, $\boldsymbol{\sigma}$ is the tensor of applied stresses, H (for history) represents symbolically the current collection of values of ξ_α, V_0 denotes the volume of a representative volume element (RVE). The summation in (2) extends over all sites of the RVE where the microstructural rearrangements take place.

Clearly, the basic prerequisite of Rice's internal variable approach, stating that material response be purely elastic when internal variables are held constant, is satisfied for frictional cracks as well. No energy is dissipated if the slip displacements and the wing crack lengths are fixed through appropriate constraints. Therefore, if the total strain increment is decomposed as

$$\mathrm{d}\boldsymbol{\varepsilon} = \mathrm{d}^e\boldsymbol{\varepsilon} + \mathrm{d}^i\boldsymbol{\varepsilon} = \mathbf{M} : \mathrm{d}\boldsymbol{\sigma} + \mathrm{d}^i\boldsymbol{\varepsilon}, \tag{3}$$

then its inelastic part is derivable from (2). The instantaneous compliance tensor M_{ijkl} is given by

$$M_{ijkl} = \left.\frac{\partial^2 \psi(\boldsymbol{\sigma}, H)}{\partial \sigma_{ij}\partial \sigma_{kl}}\right|_{H\,\text{fixed}}, \tag{4}$$

so that M_{ijkl} is symmetric on interchange of ij and kl (diagonal symmetry). In the case of *open cracks*, $\mathbf{M} = \bar{\mathbf{S}}$, where $\bar{\mathbf{S}}$ is the secant (effective) compliance, being in fact the unloading compliance. Consequently, the specific complementary energy for an elastic solid weakened by open cracks can be defined as

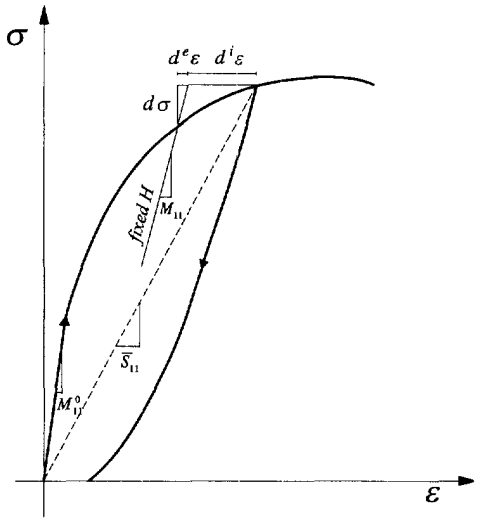

Fig. 2. Schematic ($\sigma-\varepsilon$) curve in a loading–unloading cycle of a compact rock specimen in uniaxial compression. Indicated are: initial compliance M^0_{11}, instantaneous compliance M_{11} (at fixed H), secant compliance $\bar{S}_{11}$, and actual unloading path.

$$\psi_{(\text{open cracks})} = \tfrac{1}{2}\boldsymbol{\sigma}:\bar{\mathbf{S}}:\boldsymbol{\sigma}, \tag{5}$$

with the secant compliance preserving its diagonal symmetry. However, it is a common knowledge that for Mode II *frictional sliding* the secant compliance matrix is non-symmetric (e.g., Ju, 1991, Kachanov, 1993), and hence the elastic potential defined in (5) does not exist. In this case, the secant compliance is not the unloading compliance due to frictional effects. In Fig. 2, we indicate the initial elastic compliance M^0_{11}, the secant (non-symmetric) effective compliance $\bar{S}_{11}$, the unloading path with backsliding, and the instantaneous (symmetric) compliance M_{11} given by (4). In conclusion, all basic relations of the Rice thermodynamic framework remain valid for an elastic body with frictional cracks. The only difference is that the instantaneous compliance $\mathbf{M}$ is not the secant compliance anymore. At this stage of analysis, it is just an auxiliary concept ensuing from the adopted theory. It will be shown later that $\mathbf{M}$ can unambiguously be expressed in terms of $\mathbf{M}^0$ and the wing crack length l.

2.2. *Inelastic deformation*

Phase 1 ($\mathrm{d}b > 0, l = 0, \mathrm{d}l = 0$). From the superposition principle, Fig. 3a, and from the elementary equilibrium on the initial crack plane, it follows that

$$\tau_{eff}2c + 2F_{el} = 0 \quad \text{and} \quad \sigma'_{11} = \sigma'^{r}_{11}, \tag{6}$$

where

$$\tau_{eff} = \tau'_{12} - \tau'^{r}_{12}. \tag{7}$$

In eqns (6) and (7), σ'_{11}, τ'_{12} are the normal and shear stresses *actually* acting on PP', $\sigma'^{r}_{11}, \tau'^{r}_{12}$ are the resolved normal and shear stresses on that plane, F_{el} is as yet undetermined elastic crack-closing force acting as to reverse the sliding displacement.

Frictional contact on PP' is of the Mohr–Coulomb type, i.e., τ'_{12} and σ'_{11} are related through a simple law (yield condition)

$$\tau'_{12} = \tau_c - \mu\sigma'^{r}_{11}, \tag{8}$$

where τ_c is the cohesion and μ the coefficient of dry friction. Both quantities are in fact not constants but some functions of the slip displacement $b(x'_2)$, thus they depend on the loading program. However, having in mind that the proposed constitutive theory is more

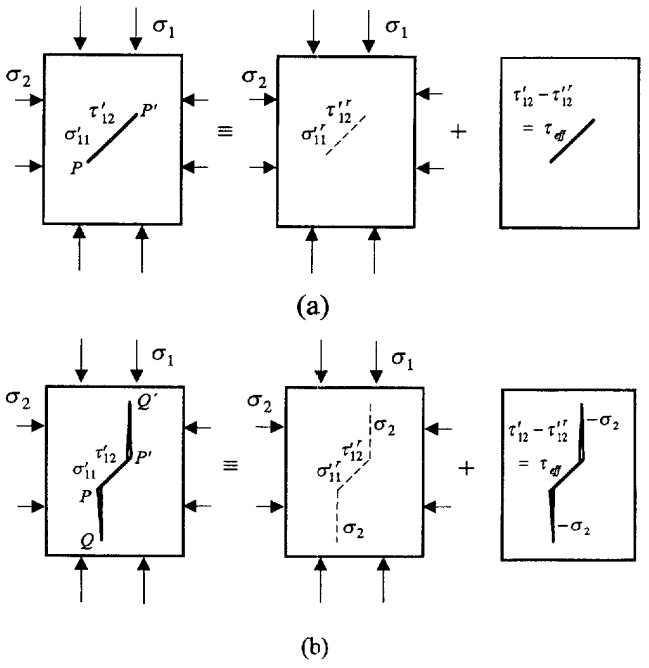

Fig. 3. Superposition of stresses: (a) phase 1, (b) phase 2.

of a qualitative character, and the variations of τ_c and μ are anyhow rather poorly documented, it is assumed that τ_c and μ are positive constants throughout. If appropriate relations determining τ_c and μ are available, they can easily be incorporated in the present framework.

Anticipating that thermodynamic forces will further be differentiated with respect to the applied stress tensor σ_{ij}, it is essential to put all three stress components σ_{11}, σ_{22}, τ_{12} in the expression for the resolved stresses in the local coordinate system (x'_1, x'_2), even though τ_{12} is actually zero. Therefore, we have

$$\begin{aligned} \sigma''_{11} &= \sigma_{11}\cos^2\varphi + \sigma_{22}\sin^2\varphi + \tau_{12}\sin 2\varphi, \\ \tau''_{12} &= -\tfrac{1}{2}(\sigma_{11} - \sigma_{22})\sin 2\varphi + \tau_{12}\cos 2\varphi, \end{aligned} \tag{9}$$

where σ_{11}, σ_{22}, τ_{12} are all negative. The effective shear stress that drives the frictional slip on PP' can now be expressed as

$$\tau_{eff} = \tau_c - \mu(\sigma_1\cos^2\varphi + \sigma_2\sin^2\varphi) + \tfrac{1}{2}\sin 2\varphi(\sigma_1 - \sigma_2). \tag{10}$$

Note that, according to (7), τ_{eff} is the shear stress along the preexisting crack as it results from the superposition principle, Fig. 3. It is negative in the local coordinate system (x'_1, x'_2) when forward sliding is activated. The average (relative) slip $\bar{b}$ of the points on PP' is equal to the average Mode II crack opening displacement induced by $(-\tau_{eff})$. Hence,

$$\bar{b} = \frac{1}{2c}\int_{-c}^{c} \frac{-\tau_{eff}(1-\nu_0^2)}{E_0}\sqrt{c^2 - x'^2_2}\,\mathrm{d}x'_2 = -\frac{\pi c\tau_{eff}(1-\nu_0^2)}{E_0}, \tag{11}$$

where E_0 is the Young modulus and ν_0 the Poisson ratio of the matrix material. From (6) and (11) it follows that the elastic crack-restoring force equals

$$F_{el} = \frac{\bar{b}E_0}{\pi(1-\nu_0^2)}. \tag{12}$$

The yield condition (8) can now be rewritten as

$$\Omega_1^s = \tau_c - \mu(\sigma_1 \cos^2\varphi + \sigma_2 \sin^2\varphi) + \frac{1}{2}\sin 2\varphi(\sigma_1 - \sigma_2) + \frac{\bar{b}E_0}{\pi c(1-\nu_0^2)} = 0. \tag{13}$$

We shall refer to (13) as the *sliding activation equation* (or yield condition) in phase 1. A similar equation was used in Moss and Gupta (1982) for some particular representation of the winged crack configuration. In their analysis, phase 1 was not considered. It can be seen that (13) predicts the onset of sliding when $\tau_{eff} = 0$.

The next step in our analysis is to determine the complementary energy for the representative surface element containing a crack that undergoes frictional sliding. Formally, the specific complementary energy can be decomposed as

$$\psi(\boldsymbol{\sigma}, H) = \psi^0(\boldsymbol{\sigma}) + \Delta\psi(\boldsymbol{\sigma}, H), \tag{14}$$

where: $\psi^0(\boldsymbol{\sigma}) = \frac{1}{2}\sigma_{ij}M^0_{ijkl}\sigma_{kl}$, and M^0_{ijkl} is the elastic compliance tensor of the matrix material. The inelastic part of the specific complementary energy due to frictional sliding is equal to the area average of the work done by the actual shear tractions along PP' on the slip displacements:

$$\Delta\psi(\boldsymbol{\sigma}, H) = \frac{1}{A_0}\int_{-c}^{c}\int_0^{b(x_2')} \tau_{12}'(\sigma, b)\,\mathrm{d}b\,\mathrm{d}x_2'. \tag{15}$$

If $b(x_2') = \bar{b} = \text{const.}$ then in view of (7) and (11), expression (15) takes the form

$$\Delta\psi(\boldsymbol{\sigma}, \bar{b}) = \frac{2c}{A_0}\int_0^{\bar{b}} \tau_{12}'(\boldsymbol{\sigma}, \bar{b})\,\mathrm{d}\bar{b} = \frac{1}{A_0}\left[\tau''_{12}\bar{b}2c - \frac{\bar{b}^2E_0}{\pi(1-\nu_0^2)}\right]. \tag{16}$$

Note that τ_{12}' in (16) is a function of both the applied stress and the slip displacement. Having determined $\Delta\psi$ we can compute the inelastic change of ψ:

$$\mathrm{d}^i\psi = \left.\frac{\partial(\Delta\psi(\boldsymbol{\sigma}, \bar{b}))}{\partial\bar{b}}\right|_{\boldsymbol{\sigma}\text{ fixed}} \mathrm{d}\bar{b} = \frac{1}{A_0}\tau_{12}'2c\,\mathrm{d}\bar{b}. \tag{17}$$

From (17) and (A.5) in Appendix 1, it is straightforward to identify the microflux and the conjugate force:

$$\mathrm{d}\xi_1 = \mathrm{d}\bar{b}, \quad f_1 = \tau_{12}'2c = 2c\left[\tau''_{12} - \frac{\bar{b}E_0}{\pi c(1-\nu_0^2)}\right]. \tag{18}$$

Rice (1971) proved that the normality rule holds in macroscopic constitutive laws when the rate of change of each internal variable depends on the external stresses only via its own conjugated thermodynamic force. Rephrased for the time-independent case, this statement means that the yield condition for αth internal variable is expressed only in terms of the conjugated force f_α, with the yield limits depending on H (Hill and Rice, 1973). Let us interpret these statements in the case of frictional sliding along crack faces. Evidently, the increment of frictional slip $\mathrm{d}\bar{b}$ is governed by the increment of net shear stress τ_{eff} which is different from the conjugated thermodynamic stress τ_{12}', (18). In other words, the yield condition (13) is not expressible in terms of τ_{12}' and $\bar{b}$ alone, but it also depends on the normal stress acting on the initial split PP'. Hence, in the considered case, the normality

property will not emerge in a macroscopic constitutive law. This analysis provides a micromechanical explanation of the well-known fact that the normality rule is not valid for frictional materials (e.g., Rudnicki and Rice, 1975).

By inserting the conjugate force (18) into the fundamental relation (2) and performing the required differentiation, the increment of inelastic strain in phase 1 takes the following explicit form

$$\mathrm{d}^i\varepsilon_{ij} = \omega_0 \begin{bmatrix} -\sin 2\varphi & \cos 2\varphi \\ \cos 2\varphi & \sin 2\varphi \end{bmatrix} \mathrm{d}\tilde{b}, \tag{19}$$

where: $\omega_0 = Nc^2/A_0$ is the initial crack density parameter in 2D case, N is the number of (non-interacting) cracks having the same orientation φ. Additionally, we introduce a normalized slip and a normalized wing crack length as

$$\tilde{b} = \bar{b}/c, \quad \tilde{l} = l/c. \tag{20}$$

Depending on the context, both the averaged slip $\bar{b}$ (not normalized) and its normalized counterpart $\tilde{b}$ will be used in the sequel.

To complete the analysis in phase 1, we have to relate the increment of slip displacement to the increment of stress. This can be done from the consistency condition that assures continuous forward sliding, i.e., by time-differentiation of the sliding activation eqn (13).

It is worth mentioning that the expression (19) is identical to (A.4) in Nemat-Nasser and Obata (1988), obtained on the kinematic grounds.

Phase 2 ($\mathrm{d}\tilde{b} > 0, \mathrm{d}\tilde{l} > 0$). In this phase, the entire sliding crack mechanism is operative. The energy is dissipated on the frictional sliding on preexisting flaw and on the growth of wing cracks. The exact values of the stress intensity factors (SIFs) at the tips of curvilinear wing cracks can be obtained numerically by solving an appropriate singular integral equation (Horii and Nemat-Nasser, 1985). On the other hand, there exist numerous closed-form approximations for the SIFs in question in the open literature; see, for example, Moss and Gupta (1982), Zaitsev (1985), Ashby and Hallam (1986), Horii and Nemat-Nasser (1986), Kemeny and Cook (1991). A detailed analysis of the accuracy of these approximations is an interesting topic but beyond the scope of this paper. It should be though mentioned that some of these estimates are not quite correct since they predict unreasonable asymptotic crack behaviors, especially in the long-wing limit ($\tilde{l} \gg 1$). Of all these models, we selected the expressions in Horii and Nemat-Nasser (1986) since they provide good estimates of the SIFs for short and long wings alike. Assume that wedging effect and slip displacement exerts on the wings is represented by two collinear splitting forces $F = -2c\tau_{eff}$. Assume also that the curvilinear wing cracks can be approximated by straight ones whose orientation θ is yet to be determined from the maximization of K_{I}. Then, the K_{I}, K_{II} factors at Q and Q' in the crack configuration depicted in Fig. 4a are given by

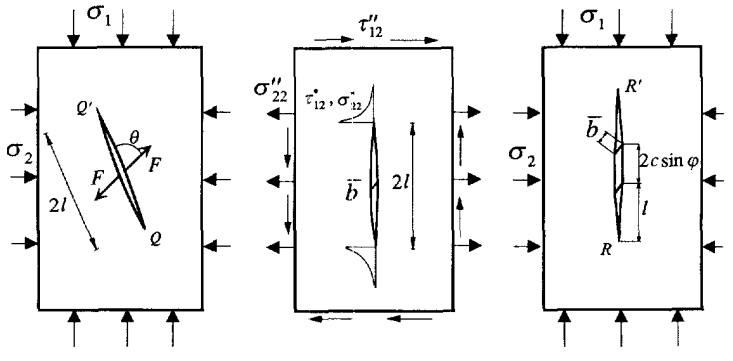

Fig. 4. (a) Representative tension crack QQ' with splitting forces. (b) Fictitious stresses σ''_{22} and τ''_{12} producing the same maximum CODs as the loads in Fig. 1. (c) Displacement-driven crack model.

$$K_{\mathrm{I}} = \frac{F\sin\theta}{\sqrt{\pi(l+l^*)}} + \sqrt{\pi l}[\sigma_{11}\cos^2(\theta+\varphi) + \sigma_{22}\sin^2(\theta+\varphi) + \tau_{12}\sin 2(\theta+\varphi)], \tag{21}$$

$$K_{\mathrm{II}} = \frac{-F\cos\theta}{\sqrt{\pi(l+l^*)}} - \sqrt{\pi l}\left[-\frac{1}{2}(\sigma_{11}-\sigma_{22})\sin 2(\theta+\varphi) + \tau_{12}\cos 2(\theta+\varphi)\right], \tag{22}$$

where $l^* = 0.27c$ was introduced in Horii and Nemat-Nasser (1986) to render K_{I} and K_{II} non-singular at $l = 0$. Horii and Nemat-Nasser's formulas, originally written for the principal compressive stresses σ_1, σ_2, are extended here to a general two-dimensional state of stress in view of a subsequent differentiation operation in (2).

To facilitate further analysis, the actual curvilinear wing will, from now on, be approximated by a *straight* opened crack growing parallel to the direction of maximum principal compression stress σ_1. This assumption is more than justified for long wings since, according to all available experimental data, indeed $\theta \to (90^\circ - \varphi)$ as σ_1 increases. When the wings are short, this assumption overestimates SIFs at Q and Q' leading in the extreme case ($l \to 0$) to stress singularity. On the other hand, already for the wing length as small as $\tilde{l} = 1$, the corresponding difference in K_{I} is merely 11.3%. As for the inelastic strains, this effect is even less consequential since $\tilde{b}$ (to which inelastic strains are proportional) is small itself. Finally, and most importantly, we emphasize a qualitative aspect of the present study that warrants such a simplification.

The SIFs (21) and (22) now take the much simpler form

$$K_{\mathrm{I}} = \frac{F\cos\varphi}{\sqrt{\pi l}} + \sigma_{22}\sqrt{\pi l}, \tag{23}$$

$$K_{\mathrm{II}} = \frac{-F\sin\varphi}{\sqrt{\pi l}} + \tau_{12}\sqrt{\pi l}, \tag{24}$$

where $F = -2c\tau_{eff}$ as before.

Equilibrium equations in the cross-section $QPP'Q'$ (Fig. 3b) and the Mohr–Coulomb condition (8) for the relative motion of the preexisting crack faces, are now combined to yield the sliding activation equation in phase 2:

$$\Omega_2' = \tau_{eff} + \tau_{12}\tilde{l}\sin\varphi - \sigma_{22}\tilde{l}\cos\varphi + \hat{F}_{el}(\tilde{b},\tilde{l}) = 0, \tag{25}$$

where $\hat{F}_{el}(\tilde{b},\tilde{l}) = F_{el}^{\mathrm{I}}(\tilde{b},\tilde{l})\cos\varphi + F_{el}^{\mathrm{II}}(\tilde{b},\tilde{l})\sin\varphi$, with $F_{el}^{\mathrm{I}}(\tilde{b},\tilde{l})$ and $F_{el}^{\mathrm{II}}(\tilde{b},\tilde{l})$ being the elastic crack restoring forces in Mode I and II; the net shear stress τ_{eff} is determined by (10). Note that in (25) we balanced the forces along the line of initial slit PP'. It is here tacitly assumed that σ_{11}', entering (25) through the Mohr–Coulomb condition (8), is equal to σ_{11}''. In other words, normal stress transmitted across the closed slit is taken as unaffected by the presence of straight vertical wings.

The exact solution for $F_{el}^{\mathrm{I}}(\tilde{b},\tilde{l})$ and $F_{el}^{\mathrm{II}}(\tilde{b},\tilde{l})$ is contingent on the availability of stress–COD relations for the winged crack. Unfortunately, for the configuration shown in Fig. 3b, such a relation is not available in analytical form. Therefore, we have to resort to an approximate method to determine F_{el}^{I} and F_{el}^{II}. To this end, consider a representative straight crack $2l$ in an infinite plate subject to some fictitious homogeneous stresses σ_{22}'' and τ_{12}'', as shown in Fig. 4b. It is postulated that σ_{22}'' and τ_{12}'' produce the same maximum CODs on the representative crack as the actual loading would do on the winged crack (Fig. 1). Therefore,

$$2F_{el}^{I} = 2\int_{l}^{\infty} \sigma_{22}^{*}\,\mathrm{d}x_1 = \sigma_{22}''2l, \quad \tilde{b}\cos\varphi = \frac{4\sigma_{22}''\tilde{l}(1-\nu_0^2)}{E_0},$$

$$2F_{el}^{II} = 2\int_{l}^{\infty} \tau_{12}^{*}\,\mathrm{d}x_1 = \tau_{12}''2l, \quad \tilde{b}\sin\varphi = \frac{4\tau_{12}''\tilde{l}(1-\nu_0^2)}{E_0}, \tag{26}$$

with σ_{11}^{*} and τ_{12}^{*} marked in Fig. 4b. Hence, the last term in (25) becomes

$$\hat{F}_{el} = \frac{\tilde{b}E_0}{4(1-\nu_0^2)}. \tag{27}$$

This result coincides with that of Moss and Gupta (1982) obtained from somewhat different reasoning. Note that (27) makes the sliding activation equation (25) complete enabling the determination of $\tilde{b}$ (for $\tau_{12} = 0$), namely

$$\tilde{b} = \frac{4(1-\nu_0^2)}{E_0}(-\tau_{eff} + \sigma_2\tilde{l}\cos\varphi). \tag{28}$$

An alternative way to compute $\tilde{b}$ was offered in Nemat-Nasser and Obata (1988). It is based on the displacement-driven crack configuration shown in Fig. 4c. A thin rigid wedge represents now the effect the frictional sliding exerts on the wing crack. The SIFs at the tips R and R' involve complete elliptic integrals of the first and second kind, and can be found in Tada *et al.* (1985, p. 5.22). Nemat-Nasser and Obata (1988) assumed that the wings are far away from each other, so that their interaction can be neglected. Thus, two separate kink cracks each of length l can be considered. Physically, this is a realistic model only for very small kinks. In such a case, the linear elastic fracture mechanics furnishes a closed-form solution for the SIFs:

$$K_{\mathrm{I}}(\tilde{b}, l, \sigma) = \frac{E_0}{1-\nu_0^2}\frac{\tilde{b}\cos\varphi}{2\sqrt{2\pi l}} + \sigma_{22}\sqrt{\frac{\pi l}{2}},$$

$$K_{\mathrm{II}}(\tilde{b}, l, \sigma) = -\frac{E_0}{1-\nu_0^2}\frac{\tilde{b}\sin\varphi}{2\sqrt{2\pi l}} + \tau_{12}\sqrt{\frac{\pi l}{2}}, \tag{29}$$

Nemat-Nasser and Obata (1988) suggested that when the entire sliding crack mechanism is activated, the displacement-driven K_{I}, given by (29) should be equivalent to the force-driven K_{I} (23). This duality can be used for the determination of $\tilde{b}$:

$$\tilde{b} = \frac{4\sqrt{2}(1-\nu_0^2)}{E_0}\left[-\tau_{eff} + \sigma_2\tilde{l}\frac{2\pi}{\cos\varphi}\left(1-\sqrt{\frac{1}{2}}\right)\right]. \tag{30}$$

It can be seen that (30) and (28) exhibit the same functional dependence on τ_{eff}, σ_2 and $\tilde{l}$ to within some constants.

The inelastic portion of the specific complementary energy in phase 2 can be written as

$$\Delta\psi(\boldsymbol{\sigma}, H) = \frac{2c}{A_0}\int_0^{\tilde{b}} \tau_{12}'\ (\boldsymbol{\sigma}, \bar{b})\,\mathrm{d}\bar{b} + \frac{2}{A_0}\int_0^{l} G(\boldsymbol{\sigma}, l)\,\mathrm{d}l. \tag{31}$$

Here, τ_{12}' is to be computed balancing the forces and act in the cross section $QPP'Q'$ (the last element of the superposition diagram in Fig. 3b). This is done using (25) in which we

substitute (7) for τ_{eff}. The elastic energy release rate G equals $(1-\nu_0^2)(K_I^2+K_{II}^2)/E_0$, with K_I and K_{II} given by (23) and (24). The inelastic change of $\psi(\sigma, H)$ is

$$d^i\psi = \frac{\partial(\Delta\psi)}{\partial\tilde{b}}d\tilde{b} + \frac{\partial(\Delta\psi)}{\partial l}dl = \frac{1}{A_0}(\tau'_{12}2c\,d\tilde{b} + 2G\,dl) = \frac{1}{A_0}(f_1\,d\xi_1 + 2f_2\,d\xi_2), \tag{32}$$

where the factor 2 in the last term accounts for two crack tips. From (31) and (32), the thermodynamic forces conjugate to $d\tilde{b}$ and dl are

$$f_1 = \tau'_{12}2c = 2c[\tau''_{12} - \tau_{12}\tilde{l}\sin\varphi + \sigma_{22}\tilde{l}\cos\varphi - \hat{F}_{el}(\tilde{b}, \tilde{l})], \quad d\xi_1 = d\tilde{b}, \tag{33}$$

$$f_2 = G = \frac{1-\nu_0^2}{E_0}(K_I^2 + K_{II}^2), \quad d\xi_2 = dl. \tag{34}$$

According to Rice (1975, 1978), for Griffith cracks without forking or branching, the thermodynamic crack tip extension force per unit length is $(G-2\gamma)$. The term 2γ is the work of *reversible* separation of the fracturing surfaces. However, in the reality the surface free energy γ is practically not recoverable. Consequently, γ has been dropped in the expression for f_2, in (34). Whether or not $\gamma = const.$ is included in f_2 has no consequence on the computation of the strain.

After some computational effort, the inelastic part of a strain increment is derived to be

$$d^i\varepsilon_{ij} = \frac{N}{A_0}\left(\frac{\partial f_1}{\partial\sigma_{ij}}d\tilde{b} + 2\frac{\partial f_2}{\partial\sigma_{ij}}dl\right) = \omega_0\begin{bmatrix}-\sin 2\varphi & \cos 2\varphi \\ \cos 2\varphi & \sin 2\varphi\end{bmatrix}d\tilde{b}$$
$$+\omega_0\begin{bmatrix}0 & -\sin\varphi \\ -\sin\varphi & 2\cos\varphi\end{bmatrix}\left(\tilde{l}\,d\tilde{b} - \frac{4(1-\nu_0^2)}{E_0}\tau_{eff}\,dl\right) + \frac{4\pi\omega_0(1-\nu_0^2)}{E_0}\begin{bmatrix}0 & 0 \\ 0 & \sigma_2\end{bmatrix}\tilde{l}\,d\tilde{l}, \tag{35}$$

where, as before, $\omega_0 = Nc^2/A_0$.

We want to stress the point that certain caution is advisable when differentiating the conjugate forces with respect to the applied stress in (35). This differentiation is to be carried out at fixed H, i.e., at $\tilde{b}$ and $\tilde{l}$ held constant. In the present model, the effect of frictional sliding along PP' is represented by the action of two collinear splitting forces F. Once the internal variables $\tilde{b}$ and $\tilde{l}$ are frozen, so are the splitting forces F. Therefore, the physical law (8) or its extended version (10), defining the effective shear stress in terms of the applied stresses, should not be substituted in the expressions for the SIFs (23), (24) prior to the differentiation operation in (35). Otherwise, an incorrect solution for the inelastic strains may follow, as in Kemeny and Cook (1991). This issue is further elaborated in Appendix 2.

It is interesting to compare our result (35) with the corresponding expression in Nemat-Nasser and Obata (1988), obtained from kinematic considerations. Their formula (2.15), when specified for long wings ($d\theta = 0$) and rewritten in a comparable form, reads

$$d^i\varepsilon_{ij} = \omega_0\begin{bmatrix}-\sin 2\varphi & \cos 2\varphi \\ \cos 2\varphi & \sin 2\varphi\end{bmatrix}d\tilde{b} + \omega_0\begin{bmatrix}0 & -\sin\varphi \\ -\sin\varphi & 2\cos\varphi\end{bmatrix}\tfrac{1}{2}(\tilde{l}\,d\tilde{b} + \tilde{b}\,d\tilde{l})$$
$$+\frac{2\pi\omega_0(1-\nu_0^2)}{E_0}\begin{bmatrix}0 & 0 \\ 0 & \sigma_2\end{bmatrix}\tilde{l}\,d\tilde{l}. \tag{36}$$

First of all, we notice that the general structure of either solution is very similar. However, a closer look reveals certain differences. The first terms in (35) and (36) are the same. The last term in (35) is twice as large as the last term in (36). This difference can easily be explained if one notices that a single crack having a total length $2\tilde{l}$ (present model) responds

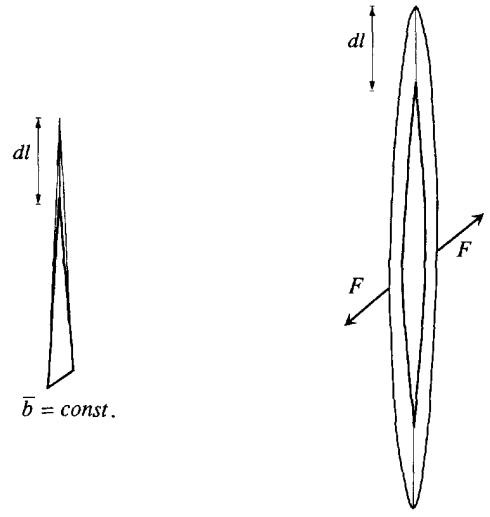

Fig. 5. (a) Graphical representation of the inelastic strain increment in (36) involving $((1/2)\tilde{b}\,\mathrm{d}\tilde{l})$ term. (b) Additional normal and shear strain increments as in (35) resulting from the force-driven model.

differently to applied loads than two separate wing cracks each of length $\tilde{l}$ (Nemat-Nasser and Obata's model), see Appendix 3.2. This difference appears in the elastic (cf. Section 2.3) and inelastic strains alike. Comparison of the second term in (35) with the corresponding term in (36) needs a somewhat extended comment. To this end, we have to express τ_{eff} as a function of $\tilde{b}$ from (28) or (30). For example, if (30) is used, the term in question becomes

$$\left[\frac{1}{2}(2\tilde{l}\,\mathrm{d}\tilde{b}+\sqrt{2}\tilde{b}\,\mathrm{d}\tilde{l})-\frac{16\pi(1-\nu_0^2)}{E_0\cos\varphi}\left(1-\sqrt{\frac{1}{2}}\right)\sigma_2\tilde{l}\,\mathrm{d}\tilde{l}\right]. \tag{37}$$

It is seen that in comparison with (36), the expression (37) contains an extra term that is proportional to $\sigma_2\tilde{l}\,\mathrm{d}\tilde{l}$. This can be explained as follows. If $\tilde{b}$ is held constant while crack length changes by $\mathrm{d}\tilde{l}$, then in the kinematic model of Nemat-Nasser and Obata the inelastic part of the strain increment is just proportional to $\tilde{b}\,\mathrm{d}\tilde{l}$. In our stress-driven model (Fig. 5), there are additional normal and shear inelastic strain increments, induced by that part of the concentrated force F which depends on $\tilde{l}$.

This first term in the first parenthesis of (37) accounts for the influence of the wing presence on the amount of strain induced by frictional sliding along preexisting cracks. This term differs by a factor of 2 from the corresponding term in (36). However, Nemat-Nasser and Obata's result, obtained for two separate (displacement driven) wing cracks, is strictly valid only in the short wing limit, and will be larger as the wings keep growing. In the present analysis, no particular model has been introduced yet for the computation of the sliding related strains. The examined term was obtained from the equilibrium of the winged crack and the fundamental relation (2). Finally, the factor $\sqrt{2}$ accompanying $\tilde{b}\,\mathrm{d}\tilde{l}$ in (37) is due to different predictions of strains furnished by F-driven vs $\bar{b}$-driven model. This issue is discussed in detail in Appendices 3.1 and 3.2.

To obtain the $(\mathrm{d}\sigma_{ij}-\mathrm{d}\varepsilon_{ij})$ relation, it remains yet to express kinematic quantities $\tilde{b}$, $\tilde{l}$ and $\mathrm{d}\tilde{b}$, $\mathrm{d}\tilde{l}$ in (35) in terms of σ_{ij} and $\mathrm{d}\sigma_{ij}$. This has already been done for $\tilde{b}$ in (28) or, alternatively, in (30). The other equation, relating $\tilde{l}$ to σ_{ij}, is provided by the Griffith crack instability condition. It is assumed that a long wing crack is subjected to pure Mode I conditions. Consequently, the crack instability condition is

$$K_{\mathrm{I}} = K_{IC}. \tag{38}$$

Hence, the normalized crack length computed from (38) and (23) is

$$\tilde{l} = (K_{IC}^2 + 4\tau_{eff}\sigma_2 \cos\varphi - K_{IC}\sqrt{K_{IC}^2 + 8c\tau_{eff}\sigma_2 \cos\varphi})/(2\pi c\sigma_2^2). \tag{39}$$

2.3. *Elastic strains*

The description of deformation in loading regime is now completed by the computation of elastic strains. The elastic part of the total strain increment is defined in (3) with the instantaneous compliance given by (4).

In phase 1, the Gibbs potential is expressed by (14) and (16). Hence, after differentiating ψ twice with respect to $\boldsymbol{\sigma}$, it follows that

$$M_{ijkl} = M^0_{ijkl}. \tag{40}$$

This result means that friction on preexisting cracks of a fixed length ($2c$) does not change the instantaneous compliance if the friction coefficient remains constant during deformation.

In phase 2, the Gibbs potential is expressed by (14) and (31). Inserting the formulas for the F-driven SIFs (23), (24) into (31), and carrying out the differentiation in (4), we obtain

$$\begin{aligned} M_{ijkl} &= M^0_{ijkl} + \frac{1-\nu_0^2}{E_0}\frac{2N}{A_0}\int_0^l \frac{\partial^2}{\partial\sigma_{ij}\,\partial\sigma_{kl}}(K_{\mathrm{I}}^2 + K_{\mathrm{II}}^2)\,\mathrm{d}l \\ &= M^0_{ijkl} + \frac{1-\nu_0^2}{E_0} 2\pi\omega_0 l^2[\delta_{i2}\delta_{j2}\delta_{k2}\delta_{l2} + \frac{1}{4}(\delta_{i1}\delta_{j2} + \delta_{i2}\delta_{j1})(\delta_{k1}\delta_{l2} + \delta_{k2}\delta_{l1})]. \end{aligned} \tag{41}$$

If the same computation is repeated using the $\tilde{b}$-driven SIFs (29), factor 2 in front of the square bracket in the last term of (41) vanishes. This again stems from the fact that in the F-driven model a single crack of length $2l$ is considered whereas in the $\tilde{b}$-driven model two separate wing cracks emerge, each of the length l (Appendix 3.2).

2.4. *Unloading*

So far our analysis was concerned with the loading regime. Consider now unloading by *reducing* the applied stresses. It should be emphasized that for sliding cracks, reduction of applied stresses does not necessarily mean elastic unloading. The energy may locally be dissipated on backsliding or wing growth of some cracks despite the fact that the overall stress is actually decreasing. In the present model a winged crack is considered 'unloaded' if its effective shear stress changes such that $\mathrm{d}|\tau_{eff}| < 0$. Depending on the load path, various situations may take place, namely:

- *sliding crack mechanism is locked*; this may happen when axial stress dropped but insufficiently to initiate backsliding (or wing growth, if wings are curvilinear) while lateral confinement remains constant,
- *backsliding occurs without wing crack closure*; this is expected when axial stress is reduced far enough to initiate reverse sliding on a preexisting crack while lateral pressure remains unchanged; backsliding is driven by the maximum effective shear stress accumulated within the system at the end of loading regime,
- *wing crack partially closes without backsliding*; it may happen, for instance, when axial stress is held constant while lateral confinement grows but not enough to initiate backsliding,
- *wing crack partially closes with backsliding*;
- *wing crack grows without forward sliding*; this is observed when σ_1 is held constant while lateral confinement is reduced but not enough to trigger forward sliding; it may also

happen when a real winged crack with curved wings is locked at σ_2 held constant while axial stress is reduced.

The cases will now be systematically interpreted within the present framework.

Locked crack ($\mathrm{d}\tilde{b} = 0, \mathrm{d}\tilde{l} = 0$). There is no energy dissipation when the sliding crack mechanism is locked. Hence, unloading in this case is a purely elastic process. However, in comparison with the initial (unstressed) state, the material is now slightly more compliant in the lateral direction, as predicted by (41). This behavior is to be traced back to the growth of axial wing cracks during the loading regime. Within the framework of the long-wing model, the axial compliance remains unaffected.

Backsliding without wing crack closure ($\mathrm{d}\tilde{b} < 0, \mathrm{d}\tilde{l} = 0$). As soon as the applied axial stress is reduced, the opposing forces of friction and cohesion change sign. The maximum effective shear stress attained at the end of the loading regime is accumulated as a spring force in a locked crack. At some instant in unloading, this force overcomes a cooperative resistance of friction, cohesion, and the actual shear stress on PP' so that backsliding may commence. The backsliding activation equation has the same form as the forward sliding activation eqn (25), except for the signs of cohesive and frictional stresses. The maximum crack restoring force $\hat{F}_{el}^{M}$ is to be computed from the forward sliding activation eqn (25) at the end of the loading process. In consequence, the onset of backsliding takes place when

$$(\tau'^{rM}_{12} - \tau'^{r}_{12}) + \mu(\sigma'^{rM}_{11} + \sigma'^{r}_{11}) + (\sigma^{M}_{22} - \sigma_{22})\tilde{l}^{M}\cos\varphi - (\tau^{M}_{12} - \tau_{12})\tilde{l}^{M}\sin\varphi - 2\tau_{c} = 0, \quad (42)$$

where the resolved stresses $\tau'^{r}_{12}, \tau'^{rM}_{12}, \sigma'^{r}_{11}, \sigma'^{rM}_{11}$, are given by (9), whereas $\tilde{l}^{M} = const.$ follows from the Griffith condition (38). The superscript M when assigned to a variable denotes its maximum value recorded in the loading process.

The inelastic part of strain increment comprises only two first terms of the expression (35):

$$\mathrm{d}^{i}\varepsilon_{ij} = \omega_0 \begin{bmatrix} -\sin 2\varphi & \cos 2\varphi \\ \cos 2\varphi & \sin 2\varphi \end{bmatrix} \mathrm{d}\tilde{b} + \omega_0 \begin{bmatrix} 0 & -\sin\varphi \\ -\sin\varphi & 2\cos\varphi \end{bmatrix} \tilde{l}^{M}\,\mathrm{d}\tilde{b}, \quad (43)$$

where $\mathrm{d}\tilde{b} < 0$ is obtained from (28) or (30) upon putting τ_{eff} for backsliding. It can be inferred from the structure of (43) that a permanent set remains after complete unloading both in axial and lateral direction, with the latter prevailing.

Partial crack closure without backsliding ($\mathrm{d}\tilde{b} = 0, \mathrm{d}\tilde{l} < 0$). In general, the condition for crack closure is $K_{\mathrm{I}} = 0$. In the present case, the initial crack remains locked, thus the force driven stress intensity factors (23), (24) cannot be used. It is necessary to express the SIFs in terms of $\tilde{b}, \tilde{l}$ and the applied stresses. This has been done in (29) where the sliding crack mechanism was modeled as displacement-driven. Thus, the condition for crack closure becomes

$$K_{\mathrm{I}} = \frac{E_0}{1-\nu_0^2}\frac{\tilde{b}\sqrt{c}\cos\varphi}{2\sqrt{2\pi\tilde{l}}} + \sigma_{22}\sqrt{\frac{\pi c\tilde{l}}{2}} = 0. \quad (44)$$

Using the maximum values of the slip and the wing length $\tilde{b}^{M}, \tilde{l}^{M}$ attained in loading regime we can compute the lateral confinement necessary to initiate the wing closure. If the crack closure process is to continue, the consistency relation $\dot{K}_{\mathrm{I}} = 0$ must be satisfied. Hence, as the lateral pressure increases the wing crack length decreases according to

$$\mathrm{d}\tilde{l} = \frac{E_0\tilde{b}^{M}\cos\varphi}{2\pi(1-\nu_0^2)(\sigma_2)^2}\mathrm{d}\sigma_2 < 0. \quad (45)$$

Crack closure is a non-dissipative process (crack healing is excluded). The ensuing elastic compliance tensor $\mathbf{M}$ is obtained as in (41) with the only difference that K_{I} and K_{II}

are now given by (29), in which $\tilde{b} = \tilde{b}^M$. Hence, putting $\tau_{12} = d\tau_{12} = 0$, and using (45), the strain increment in this phase becomes

$$d\varepsilon_{ij} = d^e\varepsilon_{ij} = M^0_{ijkl}\, d\sigma_{kl} + \omega_0 \frac{E_0}{4\pi(1-\nu_0^2)} \left(\frac{\tilde{b}^M}{\sigma_2}\right)^2 \cos^2\varphi \delta_{i2}\delta_{j2}\, d\sigma_2, \tag{46}$$

which is the Nemat-Nasser and Obata's (1988) result (2.28)†, obtained from the kinematic model.

Partial crack closure with backsliding ($d\tilde{b} < 0, d\tilde{l} < 0$). In this case, the backsliding activation condition and the crack closure condition (44) must be simultaneously met. The strains resulting from backsliding are inelastic, while those from wing crack closure are elastic. Both strain increments have already been computed separately in (43) and (46). However, the superscript M at $\tilde{b}^M$ in (46) has to be dropped now since the backsliding is already activated, i.e., $\tilde{b}$ is not constant anymore. The reverse slip $\tilde{b}$ and its increment $d\tilde{b}$ can be computed from (28) or (30) putting τ_{eff} modified for the backsliding circumstances. The crack length $\tilde{l}$ and its negative increment $d\tilde{l}$ are derivable from the crack closure condition (44).

Wing crack growth without forward sliding ($d\tilde{b} = 0, d\tilde{l} > 0$). This is also a macroscopic unloading case, since $|\sigma_{22}|$ decreases. If the winged crack is locked, the displacement-driven SIFs (29) are relevant. The derivation of $d^i\varepsilon_{ij}$ is similar to that of phase 2 without forward sliding. Omitting the fine details, we finally have

$$d^i\varepsilon_{ij} = \frac{N}{A_0} 2\frac{\partial G}{\partial \sigma_{ij}} dl = \frac{\omega_0}{2} \begin{bmatrix} 0 & -\sin\varphi \\ -\sin\varphi & 2\cos\varphi \end{bmatrix} \tilde{b}^M\, d\tilde{l} + \frac{(1-\nu_0^2)}{E_0} 2\pi\omega_0 \begin{bmatrix} 0 & 0 \\ 0 & \sigma_{22} \end{bmatrix} \tilde{l}\, d\tilde{l}, \tag{47}$$

where $\tilde{l}$ and $d\tilde{l}$ are to be computed from the crack growth condition (38).

3. ILLUSTRATIVE EXAMPLE

In this section, we shall illustrate the capability of the developed theoretical model to reproduce experimentally observed response of rocks under compression. For this purpose, we selected the test data obtained by Zoback and Byerlee (1975) for Westerly granite specimens subject to uniaxial compression. The Westerly granite is a relatively homogeneous and nearly brittle, compact rock whose properties and mechanical behavior are thoroughly known in rock mechanics. Thus, it seemed to be a logical choice for the comparative studies of this section.

Since crack interactions are not included, the overall stresses and strains may fairly well be approximated by simple area averages of the contributions of individual sliding cracks. Assuming a finite number of specific orientations of preexisting cracks, the average strain increment may be computed as in Nemat-Nasser and Obata (1988), from

$$d\bar{\varepsilon}_{ij} = \frac{1}{R}\sum_{r=1}^{R} d\varepsilon_{ij}(\varphi_r, \omega_0(\varphi_r)), \tag{48}$$

where R is the number of considered orientations φ_r. The strain increments under the summation sign in (48) are given by (19), (35) in loading, and (43), (46), (47) in unloading. In the example to follow, an isotropic distribution of preexisting cracks is assumed, i.e. all crack orientations are likely to appear. From the symmetry arguments, it further follows that the shear strains in the global coordinate system (x_1, x_2) must vanish.

The following material parameters were used in computations:

† To within a simplification introduced in their (E.4) and commented on thereafter.

$$E_0 = 58{,}000\ \text{MPa}, \quad \nu_0 = 0.23, \quad \sigma_{uc} = -204\ \text{MPa},$$
$$\mu = 0.65, \quad c = 5 \cdot 10^{-4}\ \text{m}, \quad K_{IC} = 0.7\ \text{MPa}\sqrt{\text{m}},$$
$$\tau_c = 12\ \text{MPa}, \quad \omega_0 = 0.375, \quad R = 90. \tag{49}$$

In (49), the numerical values of E_0, ν_0, σ_{uc} were read off from the test curves in Zoback and Byerlee (1975); see also Costin (1983). Note that σ_{uc} stands here for the highest compressive stress recorded in loading. The friction coefficient μ, the average initial crack half-length c, and the fracture toughness K_{IC} were estimated using the values for Westerly granite reported in Moss and Gupta (1982), Costin (1983), Jaeger and Cook (1979), Nemat-Nasser and Obata (1988). As was mentioned in Section 2.2, the cohesive strength τ_c was considered constant during the deformation process. The assigned value 12 MPa is just the arithmetic mean between the initial cohesion $\tau_c^0 = 24$ MPa given in Moss and Gupta (1982), and the $\tau_c = 0$ (to be expected after a sufficient amount of slip displacement has been accumulated). No experimental data were available with regard to the initial microcrack density parameter $\omega_0 = Nc^2/A_0$. The selected value provided the best fit with the experimental data, and is rather consistent with those assumed in Moss and Gupta (1982) and Nemat-Nasser and Obata (1988).

The solid curves depicted in Fig. 6a, b represent the $(\sigma - \varepsilon)$ equations predicted by the present model, while dots are the experimental results measured by Zoback and Byerlee (1975) on cylindrical specimens in uniaxial compression. Since the initial closure of voids was not accounted for, the computed $(\sigma - \varepsilon)$ curve was shifted from the original 0 by the strain obtained from the intercept of the linear portion of the experimental curve with the ε-axis. It can be seen in Fig. 6a, b that the agreement between theoretical and experimental results is fairly good both in loading and unloading regime, although it was not sought. However, this agreement should be taken with caution because the experimental data are for cylindrical specimens, whereas the model is two-dimensional. In any case, a simple damage model presented in this paper does predict several important features of the brittle response of granite: the overall trends in loading and unloading are well preserved, the lateral inelastic strain is substantially larger than its axial counterpart, the permanent set and hysteresis loops are accounted for. Note that the material parameters (49) used in the computations are realistic and are documented in the referenced literature. Typically of micromechanical models, the present formulation contains no fitting parameters. All the involved parameters have clear physical meaning, although their numerical values may not always be available in the existing literature.

4. COMMENT ON CRACK INTERACTIONS AND SOFTENING BEHAVIOR

In this section we briefly outline how the crack–crack interactions can be incorporated into the present thermodynamic framework. The proposed algorithm is illustrated on the example of phase 1 cracks (cf. Section 2.2). A detailed analysis of the winged crack interactions and its subsequent embodying into the Rice formalism is the topic of current studies and will be reported in a separate paper. Of several direct methods dealing with crack–crack interactions (e.g. Gross, 1982; Horii and Nemat-Nasser, 1985; Benveniste *et al.*, 1989), the one proposed by Kachanov (1987) is chosen for its simplicity and accuracy.

Within the present framework, the crack interaction effects (amplification or shielding) will influence the thermodynamic forces and the fluxes. In phase 1 it suffices to determine the average actual shear traction (conjugate force) τ'_{12} along the preexisting crack, and the average slip displacement (internal variable) $\bar{b}$ from which the inelastic strains can be computed in a standard manner of Section 2.2. The average (actual) normal traction and the average net shear stress (7) acting on the αth crack can be represented as follows

$$\sigma'_{11} = \sigma'^{r}_{11} + \Delta\sigma'_{11},$$
$$\tau_{eff} = \tau'_{12} - (\tau'^{r}_{12} + \Delta\tau'_{12}), \tag{50}$$

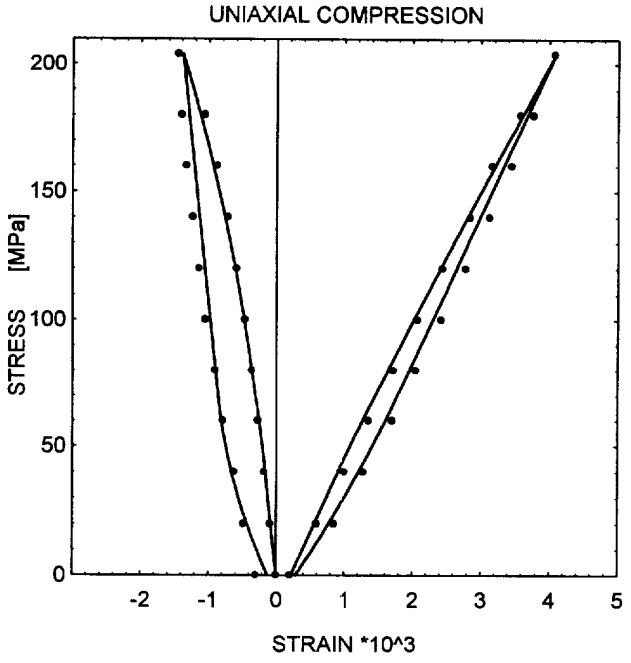

(a)

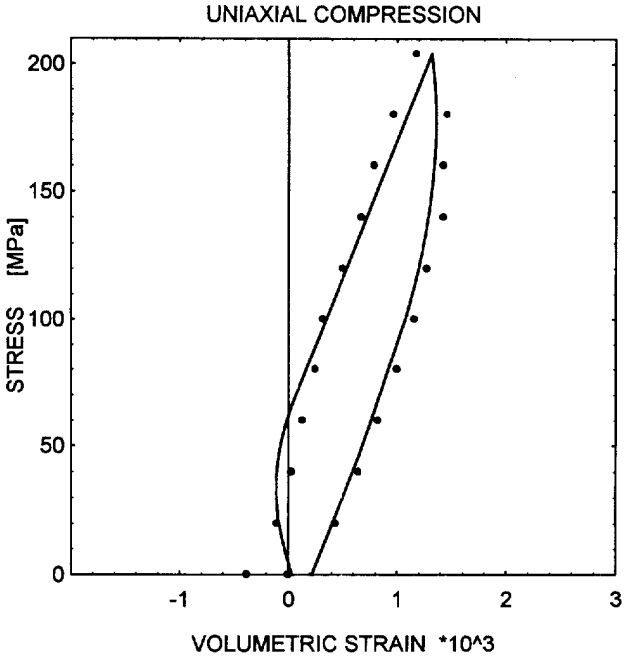

(b)

Fig. 6. Analytical results (solid curves) vs experimental data (Zoback and Byerlee, 1975) for Westerly granite in uniaxial compression: (a) axial and lateral ($\sigma-\varepsilon$) curves; (b) volumetric strains.

where $\Delta\sigma'_{11}$, $\Delta\tau'_{12}$ denote the additional average normal and shear stresses caused at the site of the αth crack in a continuous material by the other cracks (interaction terms). These stresses can be determined assuming that the average COD vector on a given crack is approximately proportional to the average traction vector on this crack (Kachanov, 1987)

$$\Delta t_i^{\alpha} = \frac{E_0}{\pi(1-\nu_0^2)} \Lambda_{ij}^{\beta\alpha} \tilde{b}_j^{\beta} \quad (\text{sum over } \beta = 1, \ldots, N; \quad \beta \neq \alpha), \tag{51}$$

where $\Delta \mathbf{t}^{\alpha} = (\Delta\sigma'_{11}, \Delta\tau'_{12})^{\alpha}$ is the additional average traction vector (at the site of the αth crack in a continuous material) induced by all other cracks, $\tilde{\mathbf{b}}^{\beta}$ is the average displacement discontinuity vector on the βth crack (normalized with respect to the crack half length c^{β}), $\Lambda^{\beta\alpha}$ are the transmission factors (Kachanov, 1987). Once the interaction term in $(50)_2$ is known, the thermodynamic force $f_1 = \tau'_{12} 2c$ can be obtained much in the same way as shown in Section 2.2 for non-interacting cracks. As for the slip displacement, the sliding activation eqn (13) must be modified to become

$$(\tau'^{r}_{12} - \tau_c + \mu\sigma'^{r}_{11})^{\alpha} + (\mu\Delta\sigma'_{11} + \Delta\tau'_{12})^{\alpha} - \frac{\tilde{b}^{\alpha} E_0}{\pi(1-\nu_0^2)} = 0. \tag{52}$$

Combining (51) and (52) and recognizing that the first term in (52) represents the net shear stress in the case without crack interactions, we obtain the following system of linear equations from which $\tilde{b}^{\alpha}$ can be determined

$$(\tau^{\alpha}_{eff})_{(\text{no interaction})} - \frac{E_0}{\pi(1-\nu_0^2)} \sum_{\beta=1}^{N} [(1-\delta^{\beta\alpha})\Lambda_{ij}^{\beta\alpha}(-\mu\mathbf{n}_i + \mathbf{m}_i) - \delta^{\beta\alpha}\mathbf{m}_j]\tilde{b}_j^{\beta} = 0, \quad (\alpha = 1, \ldots, N) \tag{53}$$

where $\mathbf{n}$, $\mathbf{m}$ are the unit vectors normal and tangential to the crack line, respectively. Determination of the thermodynamic forces and fluxes in phase 2, although feasible, is far more complicated. It requires a further extension of the Kachanov scheme to the force-driven or displacement-driven (straight crack) models of the winged crack.

When the affinities and fluxes are defined and the kinetic equations for the fluxes are provided, the constitutive model with the built-in crack interaction effects is completed. It can be next used in different applications, one being the analysis of localization of deformations in brittle materials. It was shown by Rudnicki and Rice (1975), Rice (1976) that the onset of localization is very sensitive to the details of a constitutive law. Consequently, it is expected that the crack interaction will affect the localization conditions. This issue can be examined on the basis of the present micromechanical model once the crack interaction effects are included. However, the phenomena beyond the localization threshold (softening behavior) cannot be analyzed within the Rice internal variable framework. Rice's framework requires that strain be macroscopically homogeneous (Rice, 1971) which is obviously not the case in the softening regime.

5. CLOSURE

The principal objective of this paper was to explore the issue of applicability of the Rice internal variable thermodynamic framework to the constitutive description of damaged *brittle* solids under proportional or non-proportional compressive stresses. Special attention was paid to the transition from structural rearrangements on the microscale to the macroscopic inelastic strain, when the dominant mechanism of inelastic deformation was that of the sliding crack. The microfluxes and the conjugated forces were unambiguously identified in loading and unloading regimes. Incremental nonlinear stress–strain relations were derived and the kinetic equations for the slip displacement and the wing crack length were given. It was explicitly shown in terms of micromechanics, why the normality property does not hold in macroscopic constitutive equations for frictional materials.

The $(d\sigma_{ij} - d\varepsilon_{ij})$ equations derived in this paper are very similar to those of Nemat-Nasser and Obata (1988) obtained from the kinematic analysis. The minor differences were traced back to the assumed simplifications in modeling. In particular, the differences

inherent in the stress-driven vs displacement-driven model of the basic mechanism were pointed out (Appendix 3).

The presented model is strictly valid for the long wing approximation. The short wing limit with the initial curvilinear path of the wing tips is considered elsewhere (Basista and Gross, submitted).

Preliminary developments indicate that the model can be extended to include strong interaction effects of winged cracks using the method of Kachanov (1987). It was shown on the example of straight frictional cracks that the transmission factors appear in a straightforward manner in the internal variable framework.

The limited effort of this study left few aspects of the model still open. For example, the averaging procedure should include more realistic distributions of crack sizes and orientations. Also, the kinked crack mechanism seems to be suitable for compact, low-porosity crystalline rocks. Models emphasizing cracks emanating from compressed voids may be more adequate for less-compact, sedimentary rocks of inferior strength. Thus, other deformational mechanisms including crack interaction effects should be incorporated in the present micro-to-macro transition framework in order to establish a reasonably general analytical tool for analyses of rock deformation. Finally, the model should be extended to a three-dimensional case.

Acknowledgements—The first author gratefully acknowledges a research scholarship from the Alexander von Humboldt Foundation which made this work possible. A partial support from the Polish Committee for Scientific Research (Grant no. 7 TO 7A 026 08) is also acknowledged. Discussions with D. Krajcinovic, H. Petryk, Th. Seelig and numerical assistance of J. Korelc are appreciated.

REFERENCES

Ashby, M. F. (1979) Micromechanics of fracture in static and cyclic failure. In *Fracture Mechanics*, ed. R. A. Smith, pp. 1–27. Pergamon Press, Oxford.

Ashby, M. F. and Hallam, S. D. (1986) The failure of brittle solids containing small cracks under compressive stress states. *Acta Metallica* **34,** 497–510.

Basista, M. and Gross, D. (1997) Internal variable representation of microcrack induced inelasticity in brittle materials (submitted).

Benveniste, Y., Dvorak, G. J., Zarzour, J. and Wung, E. C. J. (1989) On interacting cracks and complex crack configurations in linear elastic media. *International Journal of Solids and Structures* **25,** 1279–1293.

Brace, W. F. and Bombolakis, E. G. (1963) A note on brittle crack growth in compression. *Journal of Geophysics Research* **68,** 709–3713.

Brace, W. F., Paulding, B. W. and Scholz, C. (1966) Dilatancy in the fracture of crystalline rocks. *Journal of Geophysics Research* **71,** 3939–3953.

Cannon, N. P., Schulson, E. M., Smith, T. R. and Frost, H. J. (1990) Wing cracks and brittle compressive fracture. *Acta Metallica Materialia* **38,** 1955–1962.

Cotterell, B. and Rice, J. R. (1980) Slightly curved or kinked cracks. *International Journal of Fracture* **16,** 155–169.

Deng, H. and Nemat-Nasser, S. (1994) Microcrack interaction and shear fault failure. *International Journal of Damage Mechanics* **3,** 3–37.

Fanella, D. and Krajcinovic, D. (1988) A micromechanical model for concrete in compression. *Engineering Fracture Mechanics* **29,** 49–66.

Hill, R. and Rice, J. R. (1973) Elastic potentials and the structure of inelastic constitutive laws. *SIAM Journal of Applied Mathematics* **25,** 448–461.

Gross, D. (1982) Spannungsintensitaetsfaktoren von Risssystemen. *Ing. Archiv* **51,** 301–310.

Horii, H. and Nemat-Nasser, S. (1985) Compression-induced microcrack growth in brittle solids: axial splitting and shear failure. *Journal of Geophysics Research* **90,** 3105–3125.

Horii, H. and Nemat-Nasser, S. (1985) Elastic fields of interacting inhomogeneities. *International Journal of Solids and Structures* **21,** 731–745.

Horii, H. and Nemat-Nasser, S. (1986) Brittle failure in compression: splitting, faulting and brittle-ductile transition. *Philosophical Transactions of the Royal Society of London* **319,** 337–374.

Ju, J. W. (1991) On two-dimensional self-consistent micromechanical damage models for brittle solids. *International Journal of Solids and Structures* **27,** 227–258.

Kachanov, M. (1982) A microcrack model of rock inelasticity, Part I: Frictional sliding on microcracks. *Mechanics of Materials* **1,** 19–27.

Kachanov, M. (1987) Elastic solids with many cracks—a simple method of analysis. *International Journal of Solids and Structures* **23,** 23–43.

Kachanov, M. (1993) Elastic solids with many cracks and related problems. *Advances in Applied Mechanics* **30,** 259–445.

Kemeny, J. M. and Cook, N. G. W. (1991) Micromechanics of deformation in rocks. In *Toughening Mechanisms in Quasi-Brittle Materials*, ed. S. P. Shah, pp. 155–188. Kluwer Academic Publishers.

Kestin, J. and Rice, J. R. (1970) Paradoxes in the application of thermodynamics to strained solids. In *Critical Review of Thermodynamics*, eds E. B. Stuart *et al.*, pp. 275–298. Mono Book Corp., Baltimore.

Krajcinovic, D., Basista, M. and Sumarac, D. (1991) Micromechanically inspired phenomenological damage model. *Journal of Applied Mechanics* **58,** 305–310.
Lockner, D. (1993) The role of acoustic emission in the study of rock fracture. *International Journal of Rock Mechanics, Minerals Science & Geomechanics Abstracts* **30,** 883–899.
Lubliner, J. (1990) *Plasticity Theory*. Macmillan Publish. Co., New York, NY.
Moss, W. C. and Gupta, Y. M. (1982) A constitutive model describing dilatancy and cracking in brittle rock. *Journal of Geophysics Research* **87,** 2985–2998.
Nemat-Nasser, S. and Horii, H. (1982) Compression-induced nonplanar crack extension with application to splitting, exfoliation and rockburst. *Journal of Geophysics Research* **87,** 6805–6821.
Nemat-Nasser, S. and Obata, M. (1988) A microcrack model of dilatancy in brittle materials. *Journal of Applied Mechanics* **55,** 24–35.
Peng, S. and Johnson, J. M. (1972) Crack growth and faulting in cylindrical specimens of chelmsford granite. *International Journal of Rock Mechanics and Minerals Science* **9,** 37–86.
Rice, J. R. (1971) Inelastic constitutive relations for solids: an internal-variable theory and its application to metal plasticity. *Journal of the Mechanics and Physics of Solids* **19,** 433–455.
Rice, J. R. (1975) Continuum mechanics and thermodynamics of plasticity in relation to microscale deformation mechanisms. In *Constitutive Equations in Plasticity*, ed. A. S. Argon, pp. 23–79. The MIT Press, Cambridge, MA.
Rice, J. R. (1976) The localization of plastic deformation. In *Proceeding 14th IUTAM Congress*, ed. W. T. Koiter, pp. 207–220. North-Holland Publ. Co., The Netherlands.
Rice, J. R. (1978) Thermodynamics of the quasi-static growth of Griffith cracks. *Journal of the Mechanics and Physics of Solids* **26,** 61–78.
Rudnicki, J. W. and Rice, J. R. (1975) Conditions for the localization of deformation in pressure-sensitive dilatant materials. *Journal of the Mechanics and Physics of Solids* **23,** 371–394.
Sadowski, T. (1994) Modelling of semi-brittle MgO ceramic behaviour under compression. *Mechanics of Materials* **18,** 1–16.
Sammis, C. G. and Ashby, M. F. (1986). The failure of brittle porous solids under compressive stress states. *Acta Metallica* **34,** 511–526.
Scholz, C. H. and Kranz, R. (1974) Notes on dilatancy recovery. *Journal of Geophysics Research* **79,** 2132–2135.
Steif, P. S. (1984) Crack extension under compressive loading. *Engineering Fracture Mechanics* **20,** 463–473.
Sumarac, D. and Krajcinovic, D. (1987) A self-consistent model for microcrack-weakened solids. *Mechanics of Materials* **6,** 39–52.
Tada, H., Paris, P. and Irwin, G. (1985) *The Stress Analysis of Cracks Handbook*. Paris Production Inc., St. Louis, MO.
Wang, R. and Kemeny, J. M. (1993) Micromechanical modeling of tuffaceous rock for application in nuclear waste storage. *International Journal of Rock Mechanics and Minerals Science & Geomechanics Abstracts* **30,** 1351–1357.
Zaitsev, Y. V. (1985) Inelastic properties of solids with random cracks. In *Mechanics of Geomaterials*, ed. Z. Bazant, Wiley, Chichester.
Zhang, A., Wagner, Ch. F., and Dresen, G. (1996) Acoustic emission, microstructure, and damage model of dry and wet sandstone stressed to failure. *Journal of Geophysics Research* (in print).
Zoback, M. D. and Byerlee, J. D. (1975) The effect of cyclic differential stress on dilatancy in Westerly granite under uniaxial and triaxial conditions. *Journal of Geophysics Research* **80,** 1526–1530.

APPENDIX 1

Consider inelastic materials that can manifest, under certain circumstances, a purely elastic response at any instant of a deformation process. A key hypothesis of the internal variable theory, advocated in Kestin and Rice (1970), Rice (1971, 1975), Hill and Rice (1973), is that every irreversible process of deformation under macroscopically homogeneous strain and temperature may be viewed as a sequence of (fictitious) constrained equilibrium states at which internal variables are somehow *frozen*, so as to have the same values as at the actual (non-equilibrium) state. Following the notation of Rice (1975), let H denote symbolically the current collection of values of (scalar) internal variables $\xi_1, \xi_2, \ldots, \xi_n$ which characterize the current microstructural state of arrangement of material constituents within a representative volume element V_0. Note that H (for *history*) can alternatively be interpreted as some memory functional recording those portions of deformation process during which inelastic response occurred. Hence, if we freeze internal variables at their instantaneous values (H fixed), the standard formalism of the equilibrium thermodynamics applies. Consequently, we can derive strain (or stress) from the thermodynamic potentials in the same way as for elastic solids, with the internal variables as parameters, i.e.,

$$\sigma_{ij} = \left.\frac{\partial \phi(\boldsymbol{\varepsilon}, H)}{\partial \varepsilon_{ij}}\right|_{H\,\text{fixed}}; \quad \varepsilon_{ij} = \left.\frac{\partial \psi(\boldsymbol{\sigma}, H)}{\partial \sigma_{ij}}\right|_{H\,\text{fixed}}, \tag{A.1}$$

where $\phi = \Phi/V_0$ is the density of the (Helmholtz) free energy, and $\psi = \Psi/V_0$ the density of the (Gibbs) complementary energy.

Since fracture and/or sliding criteria are intrinsically stress-controlled, it proves more convenient to proceed with the Rice formalism in terms of the Gibbs complementary energy.

The inelastic increment of the complementary energy density under isothermal loading conditions is defined as the change in ψ when H changes to $H + \mathrm{d}H$ while $\boldsymbol{\sigma}$ is assigned the same value:

$$\mathrm{d}^{\mathrm{i}}\psi = \psi(\boldsymbol{\sigma}, H + \mathrm{d}H) - \psi(\boldsymbol{\sigma}, H). \tag{A.2}$$

Similarly, the inelastic part of the strain increment is

$$\mathrm{d}^{i}\boldsymbol{\varepsilon} = \boldsymbol{\varepsilon}(\boldsymbol{\sigma}, H+\mathrm{d}H) - \boldsymbol{\varepsilon}(\boldsymbol{\sigma}, H). \tag{A.3}$$

If the two neighboring inelastic states, characterized by H and $H+\mathrm{d}H$, are considered as two constrained equilibrium states, then from (A.1), (A.2) and (A.3) for fixed H and $H+\mathrm{d}H$, it follows that

$$\mathrm{d}^{i}\varepsilon_{ij} = \frac{\partial(\mathrm{d}^{i}\psi(\boldsymbol{\sigma}, H))}{\partial\sigma_{ij}}. \tag{A.4}$$

The inelastic change in ψ can further be represented as

$$\mathrm{d}^{i}\psi = \frac{1}{V_0}\sum f_\alpha \,\mathrm{d}\xi_\alpha, \tag{A.5}$$

where $f_\alpha = f_\alpha(\boldsymbol{\sigma}, H)$ is a set of thermodynamic forces conjugate to the internal variables. Equation (A.5) provides the definition for the thermodynamic forces. Combining (A.5) and (A.4), we arrive at the fundamental Rice's expression relating the increments of internal variables at the microscale to the inelastic portions of strain increments:

$$\mathrm{d}^{i}\varepsilon_{ij} = \frac{1}{V_0}\sum \frac{\partial f_\alpha(\boldsymbol{\sigma}, H)}{\partial\sigma_{ij}}\mathrm{d}\xi_\alpha. \tag{A.6}$$

It is perhaps worth emphasizing that the only assumption underlying (A.6) was that of a purely elastic material response (admitting the existence of thermodynamic potentials) if the internal variables were held fixed.

The micro-to-macro transition relation (A.6) should be endowed with kinetic (evolution) equations for the rates of change of internal variables (fluxes).

$$\dot{\xi}_\alpha = r_\alpha(\mathbf{f}, H), \tag{A.7}$$

where the dot denotes time differentiation. In (A.7) $\mathbf{f}$ is a set (collectively a vector) of all thermodynamic forces on which an individual flux depends at a given level of microstructural rearrangement H. It can be shown that if $\dot{\xi}_\alpha$ is fully determined by its *own* conjugated thermodynamic force f_α, then a normality structure emerges in the macroscopic constitutive equations.

It is of some interest to mention that for elastic-brittle materials the latter property holds, i.e., a damage macropotential exists, if two conditions are satisfied in the course of deformation (Krajcinovic *et al.*, 1991): (1) microcrack interaction effects are not too strong, so that the self-consistent model for damage growth may still be used†, (2) energy losses on friction can be neglected in comparison with the energy needed for the propagation of cracks. Evidently, this is not case during the final phase of straining of rocks (splitting or localization phenomena), or if a frictional mechanism of deformation dominates on the microscale.

The kinetic equations are restricted by the second law of thermodynamics which requires that work-rate of the conjugated forces on the internal variables must be non-negative:

$$\Sigma f_\alpha \dot{\xi}_\alpha \geqslant 0. \tag{A.8}$$

This inequality does not necessarily imply that the macroscopic inelastic work-rate must always be positive (Rice, 1975, Lubliner, 1990).

APPENDIX 2

Kemeny and Cook (1991) derived nonlinear stress–strain relations for an elastic body with a single winged crack, neglecting the energy loss on friction. These authors considered the long wing approximation with the $K_I = K_{IC}$ condition for the crack growth. Their equation (15) for K_I is identical to (23) of this paper. Furthermore, they used the Castigliano theorem, i.e. essentially the same numerical operation, to compute inelastic strains due to Mode I crack propagation.

Equation (39) in Kemeny and Cook (1991) gives the inelastic strain in the *axial* direction as:

$$\varepsilon_1^i = \frac{8\omega_0 \cos\varphi(\sin\varphi\cos\varphi - \mu\cos^2\varphi)}{E_0}\left[\frac{2\tau_{eff}\cos\varphi}{\pi}\ln\tilde{l} - \sigma_2(\tilde{l}-1)\right]. \tag{A.9}$$

This result is incorrect, because there is no inelastic strain in x_1 direction if we have a pure Mode I crack growing parallel to σ_1, Fig. 4a. A closer analysis of their computations revealed the following sequence of events that had led to (A.9). In the expression (23) (of this paper), the physical law specifying the concentrated force F, i.e.,

$$F = -2c\tau_{eff} = 2c[\mu(\sigma_1\cos^2\varphi + \sigma_2\sin^2\varphi) - \tfrac{1}{2}\sin 2\varphi(\sigma_1 - \sigma_2)], \quad \tau_{cr} = 0, \tag{A.10}$$

was introduced. The Gibbs potential was next built as

† An assumption of the self-consistent model (also used in the double-embedding model and the differential scheme) is meant here that the external stress field of each microcrack does not depend on the adjacent cracks, and is approximately equal to the far-field stress.

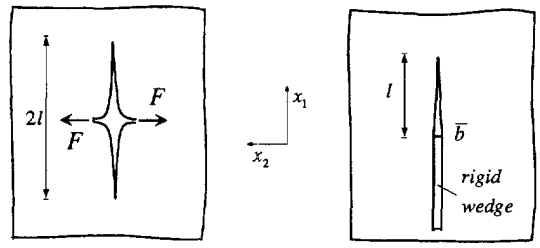

(a) (b)

Fig. A1. (a) Mode-I crack loaded by a pair of concentrated forces. (b) Mode-I crack under the action of a semi-infinite rigid wedge.

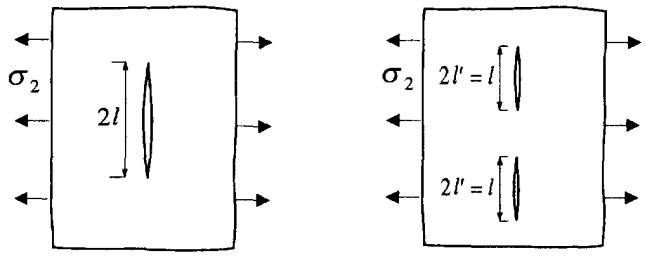

(a) (b)

Fig. A2. Crack configurations used for the computation of elastic compliances in (A.13).

$$\Delta\psi = \frac{\omega_0}{E_0} 2 \int_1^{\tilde{l}} K_I^2 \, \mathrm{d}\tilde{l} = \frac{\omega_0}{E_0} \left[\frac{8\tau_{eff}^2 \cos^2 \varphi}{\pi} \ln \tilde{l} - 8\tau_{eff}\sigma_2 \cos\varphi(\tilde{l}-1) + \sigma_2^2 \pi(\tilde{l}^2-1) \right]. \tag{A.11}$$

Finally, after expressing τ_{eff} in terms of σ_1 and σ_2 as in (A.10), the axial inelastic strain (A.9) was obtained by differentiating (A.11) with respect to σ_1. Apparently, expression (A.10), being a physical law for τ_{eff}, should not be inserted into (A.11) before the differentiation.

APPENDIX 3

It is instructive to compare the F-driven and $\bar{b}$-driven models of wing crack growth in context of resulting strains. The comparison will be done in simplest, yet relevant for the present study, cases of crack geometry and applied loads.

3.1.

Consider a Mode I crack loaded by a pair of concentrated forces shown in Fig. A.1a. Consider next a Mode I crack whose faces are pushed away by a very long, thin rigid wedge, Fig. A.1b, so that the interaction between crack tips is negligible. The force-loaded crack in Fig. A.1a has the total length $2l$. The displacement-loaded crack in Fig. A.1b consists of two cracks, each having the total length l.

Problem: assuming that $K_I(F) = K_I(\bar{b}) = K_I$, compute the inelastic strain ε_2^i in each configuration under plane strain conditions. The solution to this problem is exact and follows from the Westergaard stress functions given, for example, in Tada *et al.* (pp. 5.9, 3.11):

$$\varepsilon_2^i(F) = \frac{(1-\nu_0^2)}{A_0 E_0} 4K_I l\sqrt{\pi l}, \quad \varepsilon_2^i(\bar{b}) = \frac{(1-\nu_0^2)}{A_0 E_0} 2\sqrt{2}K_I l\sqrt{\pi l}. \tag{A.12}$$

Evidently, $\varepsilon_2^i(F) = \sqrt{2}\varepsilon_2^i(\bar{b})$.

3.2.

Consider now the crack configurations shown in Fig. A.2a,b. Assume no interaction between the two cracks in Fig. A.2b.

Problem: compute M_{22} component (Voigt notation) of the instantaneous compliance tensor $\mathbf{M}$ for the plates (representative surface elements) depicted in Fig. A.2a and Fig. A.2b. From (4), we have

$$M_{22}^{(a)} = \frac{(1-\nu_0^2)}{A_0 E_0} 2 \int_0^l 2\pi l \, \mathrm{d}l = \frac{(1-\nu_0^2)}{A_0 E_0} 2\pi l^2,$$

$$M_{22}^{(b)} = 2\frac{(1-\nu_0^2)}{A_0 E_0} 2 \int_0^{l/2} 2\pi l' \, \mathrm{d}l' = \frac{(1-\nu_0^2)}{A_0 E_0} \pi l^2. \tag{A.13}$$

It can be seen that $M_{22}^{(a)}$ is twice as much as $M_{22}^{(b)}$.

APPENDIX 4

Krajcinovic *et al.* (1991) employed the essential structure of inelastic constitutive relations (Rice, 1971, 1975) to develop a micromechanically based, *phenomenological* damage theory for brittle materials. The main results of their paper, comprising the conditions under which a damage potential exists and the identification of microfluxes, macrofluxes and conjugated thermodynamic forces, are correct. However, the specific application of the theory to a compression stress field (with the sliding crack model as the underlying micromechanism) is incorrect and should be fixed as suggested below.

If the energy losses on frictional sliding are neglected, as was assumed in Krajcinovic *et al.* (1991), the only source of energy dissipation is the growth of the wing cracks. Therefore, for a single crack in the unit cell, eqn (17) in Krajcinovic *et al.* (1991), written here in the original notation, should have the simple form

$$\dot{\psi}^* = \frac{2}{V_0} G\dot{l} = \frac{1}{2}\sigma''_{ij}\dot{S}^*_{ijkl}\sigma''_{kl}, \tag{A.14}$$

where S^*_{ijkl} is the secant compliance attributable to the presence of a crack. The fictitious stresses σ''_{ij} can be determined if the expressions for the stress intensity factors are available. Since the wings were assumed straight and collinear with the principal compressive macrostress σ_1, the expressions (23), (24) can be used. As was already discussed in Appendix 2, for vertical, straight wings growing from N isotropically distributed initial cracks, the only non-zero inelastic macrostrain component is ε^*_{22}. Consequently, the *tensile* fictitious stress σ''_2 and the lateral compliance S^*_{22} are of interest while all other components of $\mathbf{S}^*$ remain virtually unchanged. Upon requirement that K_I, given for long wings by (23) in the present paper, equals $K_I = \sigma''_2\sqrt{\pi l}$, the fictitious stresses (18) in Krajcinovic *et al.* (1991), are obtained to be

$$\begin{aligned} \sigma''_1 &= 0, \\ \sigma''_2 &= \frac{\sqrt{2}}{\pi l}\tau_{eff} + \sigma_2. \end{aligned} \tag{A.15}$$

The damage surface (expressions (19) and (25) in Krajcinovic *et al.* (1991)) can be then represented as

$$\Omega(\mathbf{Q}, H) = Q_2 - \tilde{Q}_0(H) = 0, \tag{A.16}$$

while its initial position is described by

$$\tilde{Q}_0(H) = Q_{0c} + \frac{Q_{uc} - Q_{0c}}{q^2_{uc}}(2q_{uc} - q_2)q_2. \tag{A.17}$$

In (A.16) and (A.17) $\mathbf{Q} = (1/2)(\boldsymbol{\sigma}'' \otimes \boldsymbol{\sigma}'')$, $\mathbf{q} = \mathbf{S}$. The subscripts oc and uc refer, in this case, to the onset of wing propagation and to the apex of stress–strain curve, respectively. Hence, in the uniaxial compression ($\sigma_1 = -\sigma < 0, \sigma_2 = 0$), the axial and lateral strains given by (27) in Krajcinovic *et al.* (1991) take now the following form

$$\varepsilon_{ax} = -\frac{\sigma}{E_0}, \quad \varepsilon_{lat} = \frac{\nu_0}{E_0}\sigma + q_2\sigma''_2, \tag{A.18}$$

where q_2 is to be derived from the normality property. From (A.18), it is clear that this model cannot account for the inelastic axial strains. Consequently, this is not an appropriate model for the inelastic behaviour of plain concrete, because the axial and lateral inelastic strains in concrete specimens loaded in compression are of the same order (cf. Fig. 4 in Krajcinovic *et al.*, 1991). Alternative deformational mechanisms such as the pore collapse model (Wang and Kemeny, 1993), typical of brittle materials with substantial porosity, should rather be used for concrete.

Finally, in the context of this Appendix and Section 2.1, it seems appropriate to comment that if friction is to be accounted for in a phenomenological constitutive model of a damaged elastic-brittle solid, the macroflux and the conjugated macroaffinity cannot be selected as $d\mathbf{q} = d\mathbf{S}$ and $\mathbf{Q} = (1/2)(\boldsymbol{\sigma} \otimes \boldsymbol{\sigma})$.